

Comprehensive constraints on fermionic dark matter-quark tensor interactions in direct detection experiments

Jin-Han Liang^{a,b} Yi Liao^{a,b} Xiao-Dong Ma^{a,b} Hao-Lin Wang^{a,b}

^aKey Laboratory of Atomic and Subatomic Structure and Quantum Control (MOE), Guangdong Basic Research Center of Excellence for Structure and Fundamental Interactions of Matter, Institute of Quantum Matter, South China Normal University, Guangzhou 510006, China

^bGuangdong-Hong Kong Joint Laboratory of Quantum Matter, Guangdong Provincial Key Laboratory of Nuclear Science, Southern Nuclear Science Computing Center, South China Normal University, Guangzhou 510006, China

E-mail: jinhanliang@m.scnu.edu.cn, liaoy@m.scnu.edu.cn,
maxid@scnu.edu.cn, whaolin@m.scnu.edu.cn

ABSTRACT: Effective field theory (EFT) provides a model-independent framework for interpreting the results of dark matter (DM) direct detection experiments. In this study, we demonstrate that the two fermionic DM-quark tensor operators, $(\bar{\chi}i\sigma^{\mu\nu}\gamma^5\chi)(\bar{q}\sigma_{\mu\nu}q)$ and $(\bar{\chi}\sigma^{\mu\nu}\chi)(\bar{q}\sigma_{\mu\nu}q)$, can contribute to the DM electric and magnetic dipole moments via non-perturbative QCD effects, in addition to the well-studied contact DM-nucleon operators. We then investigate the constraints on these two operators by considering both the contact and the dipole contributions using the XENON1T nuclear recoil and Migdal effect data. We also recast other existing bounds on the DM dipole operators, derived from electron and nuclear recoil measurements in various direct detection experiments, as constraints on the two tensor operators. For $m_\chi \lesssim 1$ GeV, our results significantly extend the reach of constraints on the DM-quark tensor operators to masses as low as 5 MeV, with the bound exceeding that obtained by the Migdal effect with only contact interactions by an order of magnitude or so. In particular, for the operator $(\bar{\chi}\sigma^{\mu\nu}i\gamma_5\chi)(\bar{q}\sigma_{\mu\nu}q)$ with DM mass $m_\chi \gtrsim 10$ GeV, the latest PandaX constraint on the DM electric dipole moment puts more stringent bounds than the previous direct detection limit.

KEYWORDS: Fermionic Dark Matter, Effective Field Theories, Tensor Interactions

Contents

1	Introduction	2
2	Nonperturbative matching of DM-quark interactions	4
3	XENON1T constraints	8
3.1	DM-nucleus scattering cross section	9
3.2	Constraint from NR signals	10
3.3	Constraint from the Migdal effect	11
3.4	Constraint from ER signals	13
4	Constraints from other DMDD experiments	14
5	Conclusion	15
A	Squared form factor	16

1 Introduction

Although dark matter (DM) makes up about a quarter of the total energy density of the Universe, its particle properties still remain unknown today [1, 2]. One of the theoretically motivated candidates is the weakly interacting massive particle (WIMP), which can meet the required properties to explain the DM conundrum, and at the same time, have a detectable possibility. During the past two decades, although a great amount of theoretical and experimental efforts have been dedicated to searches for the WIMPs, the DM direct detection (DMDD) experiments have not found any positive signal but constrained the DM-nucleus cross section to an unprecedented level [3, 4]. However, due to the kinematic restriction of DM-nucleus elastic scattering, the DM-nucleon interaction remains less constrained below the $\mathcal{O}(1 \text{ GeV})$ DM mass region from direct detection experiments using nuclear recoil (NR) signals. To address this limitation, inelastic processes are taken into account, for instance, bremsstrahlung processes [5] and the Migdal effect [6, 7]. Nevertheless, even with the improvement from inelastic processes, the constraints are still limited to a mass up to 40 MeV or so [8–13]. For lighter DM particles at the MeV scale, meaningful constraints require considerations like boosted DM scenarios [14, 15] or novel low-threshold detectors, see the review paper [16] and references therein. In contrast to NR experiments searching for the DM-nucleon interaction, the DM-electron interaction offers a more powerful alternative of probing low-mass DM particles through the electron recoil (ER) signal

[17, 18]. This is due to the significantly smaller mass of the electron as compared to a typical nucleus, allowing it to gain easily the recoil energy from a light DM particle. For instance, the single-electron search conducted by XENON1T has the capability of exploring a DM mass as low as approximately 5 MeV [19].

Due to the small momentum transfer (less than a few MeV) for DMDD experiments, it is preferable to adopt the low energy effective field theory (LEFT) approach to study the interactions between DM and standard model particles, which basically does not rely on the details of UV models [20–22]. The starting point for DM EFT is the DM-quark, -lepton, or -photon/gluon interactions at leading order that are color and electric charge neutral. In the Dirac DM case, the leading operators appear at dimension 5 and 6, and take the general form, $\bar{\chi}\sigma_{\mu\nu}(i\gamma_5)\chi F^{\mu\nu}$ and $(\bar{\chi}\Gamma\chi)(\bar{\psi}\Gamma'\psi)$, where χ represents the fermionic Dirac-type DM, ψ the quarks or leptons, and $F^{\mu\nu}$ the electromagnetic field strength tensor. For the interest of direct detection, ψ is usually taken to be the up, down, strange quark, and the electron. For the NR, the DM-nucleon interaction naturally arises from DM-quark and DM-gluon operators through nonperturbative matching via chiral perturbation theory (χ PT) [23].

In this work, we explore the DM-photon interactions induced by nonperturbative QCD effects from the DM-quark interactions. This will provide new ways to constrain the DM-quark interactions. Similar ideas have already been used in the study of flavor-violated radiative decays of charged leptons and neutrino electromagnetic (EM) moments [24, 25]. In particular, we consider the two tensor operators, $(\bar{\chi}i\sigma^{\mu\nu}\gamma^5\chi)(\bar{q}\sigma_{\mu\nu}q)$ and $(\bar{\chi}\sigma^{\mu\nu}\chi)(\bar{q}\sigma_{\mu\nu}q)$, which not only induce the short-distance (SD) DM-nucleon operators covered in most direct detection studies, but also generate the DM electric and magnetic dipole moment operators, $(\bar{\chi}i\sigma_{\mu\nu}\gamma_5\chi)F^{\mu\nu}$ (edm) and $(\bar{\chi}\sigma_{\mu\nu}\chi)F^{\mu\nu}$ (mdm), which also contribute to the direct detection via the long-distance (LD) photon mediator.

In previous calculations for DMDD constraints on the above two tensor operators, only the DM-nucleus scattering induced by the SD operators is considered [11, 20, 21]. In this work, we utilize the XENON1T experiment as a benchmark experiment to investigate comprehensively the constraints from both SD and LD contributions. We find that there are interesting interference effects between the two in the DM-nucleus scattering and the Migdal effect. Due to the induced dipole interactions, we also investigate the constraints from DM-electron scattering. Remarkably, owing to the excellent sensitivity to low-mass DM, the constraints from ER via this LD effect significantly extend to low-mass (from GeV to MeV) DM. In addition, we collect other existing direct detection constraints on the DM dipole operators and recast them into constraints on the DM-quark tensor operators. In our analysis, we will consider the cases of whether the flavor SU(3) symmetry is imposed or not. For the flavor conserving case, a universal Wilson coefficient is assumed for the operators involving the u, d, s quarks (here the corresponding quark mass is attached to the operator as usually practiced in the literature [23]); and for the non-conserving case,

the contributions from the three quarks are considered separately.

The paper is organized as follows. Section 2 is dedicated to nonperturbative chiral matching of the two DM-quark tensor operators onto the DM-photon and DM-nucleon interactions. We then discuss in Section 3 the constraints on these operators from the NR, the Migdal effect, and the ER, based on the XENON1T data. The full constraints and comparisons with the literature are given in Section 4. Our concluding remarks are presented in Section 5. The relevant nuclear form factors are collected in Appendix A.

2 Nonperturbative matching of DM-quark interactions

Since the transferred momentum in DMDD experiments is limited to a few hundreds of MeV, we can generically describe the interactions between DM and standard model (SM) light fields within the framework of LEFT. For DM direct detection, the complete set of operators with fermion and scalar DM particles up to canonical mass dimension 7 have been classified in [23, 26–29]. Here we are particularly interested in the two tensor operators for the Dirac fermionic DM which have not got much attention except for a few studies focusing on NR signals and the Migdal effect induced by the SD DM-nucleon interactions [11, 21]. Following the convention in [23], they are parameterized by,

$$\mathcal{O}_{\chi q}^{\text{T1}} = m_q (\bar{\chi} \sigma^{\mu\nu} \chi) (\bar{q} \sigma_{\mu\nu} q), \quad \mathcal{O}_{\chi q}^{\text{T2}} = m_q (\bar{\chi} i \sigma^{\mu\nu} \gamma_5 \chi) (\bar{q} \sigma_{\mu\nu} q), \quad (2.1)$$

where q represents the three light quarks u, d, s of mass m_q relevant to the direct detection. For each operator, there is a corresponding unknown Wilson coefficient whose magnitude is parameterized as $|C_{\chi q}^{\text{T1}(\text{T2})}| \equiv 1/\Lambda^3$ where Λ is an effective scale related to some unknown UV physics. In the following, we demonstrate that these operators not only contribute to DM-nucleon local interactions but also the DM magnetic and electric dipole moment operators, $(\bar{\chi} \sigma_{\mu\nu} \chi) F^{\mu\nu}$ and $(\bar{\chi} i \sigma_{\mu\nu} \gamma_5 \chi) F^{\mu\nu}$, through nonperturbative QCD effects. All of these contributions can be systematically extracted through matching within the framework of the (baryon) chiral perturbation theory ((B) χ PT) of QCD at low energy. For applications of (B) χ PT in the description of DM direct detection, see, for instance, Refs. [23, 30].

Our starting point is the quark level Lagrangian with external sources

$$\mathcal{L} = \mathcal{L}_{\text{QCD}} + \bar{q}_L l_\mu \gamma^\mu q_L + \bar{q}_R r_\mu \gamma^\mu q_R - [\bar{q}_R (s + ip) q_L - \bar{q}_R t^{\mu\nu} \sigma_{\mu\nu} q_L + \text{h.c.}], \quad (2.2)$$

where \mathcal{L}_{QCD} is the QCD Lagrangian for the u, d, s quarks in the chiral limit. The external sources, $l_\mu, r_\mu, s, p,$ and $t^{\mu\nu}$, are 3×3 matrices in flavor space, which contain non-strongly interacting fields like the leptons, photon, and DM that interact with quarks. For the two DM-quark interactions with a tensor quark current in Eq. (2.1), the corresponding tensor external source is given by

$$t^{\mu\nu} = P_L^{\mu\nu\alpha\beta} \bar{t}_{\alpha\beta}, \quad (2.3)$$

where the first factor on the right-hand side is a tensor chiral projection operator [31] defined as

$$P_L^{\mu\nu\alpha\beta} = \frac{1}{4} \left(g^{\mu\alpha} g^{\nu\beta} - g^{\mu\beta} g^{\nu\alpha} - i\epsilon^{\mu\nu\alpha\beta} \right), \quad (2.4)$$

and $\bar{t}^{\mu\nu}$ is related to the DM tensor currents and couplings $C_{\chi q}^{\text{T1(T2)}}$, which is a diagonal matrix in flavor space in our consideration,

$$(\bar{t}^{\mu\nu})_{qq} = C_{\chi q}^{\text{T1}} m_q (\bar{\chi} \sigma^{\mu\nu} \chi) + C_{\chi q}^{\text{T2}} m_q (\bar{\chi} i \sigma^{\mu\nu} \gamma_5 \chi). \quad (2.5)$$

The building blocks of chiral matching of the Lagrangian in Eq. (2.2) consist of the pseudo Nambu-Goldstone boson (pNGB) matrix U , the baryon octet fields B , and external sources. We begin with the pure mesonic chiral Lagrangian that will lead to DM EM moments directly. The leading order Lagrangian appears at $\mathcal{O}(p^2)$ in chiral power counting [32, 33],

$$\mathcal{L}_{\chi\text{PT}}^{(2)} = \frac{F_0^2}{4} \text{Tr} \left[D_\mu U (D^\mu U)^\dagger \right] + \frac{F_0^2}{4} \text{Tr} \left[\chi U^\dagger + U \chi^\dagger \right], \quad (2.6)$$

where F_0 is the pion decay constant in the chiral limit and U is related to the pNGBs by

$$U = \exp \left[i \frac{\sqrt{2} \Phi}{F_0} \right], \quad \Phi = \begin{pmatrix} \frac{\pi^0}{\sqrt{2}} + \frac{\eta}{\sqrt{6}} & \pi^+ & K^+ \\ \pi^- & -\frac{\pi^0}{\sqrt{2}} + \frac{\eta}{\sqrt{6}} & K^0 \\ K^- & \bar{K}^0 & -\sqrt{\frac{2}{3}} \eta \end{pmatrix}, \quad (2.7)$$

and the covariant derivative of U and the combined scalar source χ are

$$D_\mu U = \partial_\mu U - i l_\mu U + i U r_\mu, \quad \chi = 2B(s - ip). \quad (2.8)$$

The tensor source first appears at $\mathcal{O}(p^4)$ [31], which will yield the DM EM dipole moments. The relevant term is

$$\mathcal{L}_{\chi\text{PT}}^{(4)} \supset \Lambda_1 \text{Tr} \left[t_+^{\mu\nu} f_{+\mu\nu} \right], \quad (2.9)$$

where Λ_1 is a low energy constant (LEC) which is usually parameterized in terms of the chiral symmetry breaking scale Λ_χ in the form, $\Lambda_1 = c_T \Lambda_\chi / (16\pi^2)$, with c_T an unknown dimensionless constant. Here the tensor field matrices in flavor space are given by

$$t_+^{\mu\nu} = u^\dagger t^{\mu\nu} u^\dagger + u t^{\mu\nu\dagger} u, \quad f_+^{\mu\nu} = u F_L^{\mu\nu} u^\dagger + u^\dagger F_R^{\mu\nu} u, \quad (2.10)$$

with $u^2 = U$. The chiral field strength tensors read

$$F_L^{\mu\nu} = \partial^\mu l^\nu - \partial^\nu l^\mu - i[l^\mu, l^\nu], \quad F_R^{\mu\nu} = \partial^\mu r^\nu - \partial^\nu r^\mu - i[r^\mu, r^\nu]. \quad (2.11)$$

For our purpose, the vector external sources are recognized as,

$$l_\mu = r_\mu = -e A_\mu \text{diag}(Q_u, Q_d, Q_s), \quad (2.12)$$

where A_μ denotes the photon field and Q_q the electric charge of quark q in units of $e > 0$.

Expanding Eq. (2.9) to the lowest order in pNGB fields, the following DM edm and mdm interactions arise,

$$\mathcal{L}_{\chi\text{PT}}^{(4)} \supset \frac{\mu_\chi}{2} (\bar{\chi} \sigma^{\mu\nu} \chi) F_{\mu\nu} + \frac{d_\chi}{2} (\bar{\chi} i \sigma^{\mu\nu} \gamma_5 \chi) F_{\mu\nu}, \quad (2.13)$$

with the DM mdm and edm being

$$\mu_\chi = -\frac{ec_T \Lambda_\chi}{12\pi^2} \left(\sum_q 3Q_q C_{\chi q}^{\text{T1}} m_q \right) = \frac{ec_T \Lambda_\chi}{12\pi^2} (C_{\chi d}^{\text{T1}} m_d - 2C_{\chi u}^{\text{T1}} m_u + C_{\chi s}^{\text{T1}} m_s), \quad (2.14a)$$

$$d_\chi = -\frac{ec_T \Lambda_\chi}{12\pi^2} \left(\sum_q 3Q_q C_{\chi q}^{\text{T2}} m_q \right) = \frac{ec_T \Lambda_\chi}{12\pi^2} (C_{\chi d}^{\text{T2}} m_d - 2C_{\chi u}^{\text{T2}} m_u + C_{\chi s}^{\text{T2}} m_s). \quad (2.14b)$$

Assuming the DM EM dipole moments are dominated by these nonperturbative contributions, we can establish the relation between the scale $\Lambda = |C_{\chi q}^{\text{T1,2}}|^{-1/3}$ for the DM-quark tensor operators and the dipole moments via

$$\Lambda = \left| \frac{ec_T \Lambda_\chi (3Q_q m_q)}{12\pi^2} \frac{1}{\mu_\chi} \right|^{1/3} \approx 4 \text{ GeV} \left| \frac{3Q_q m_q}{2 \text{ MeV}} \frac{10^{-9} \mu_B}{\mu_\chi} \right|^{1/3}, \quad (2.15a)$$

$$\Lambda = \left| \frac{ec_T \Lambda_\chi (3Q_q m_q)}{12\pi^2} \frac{1}{d_\chi} \right|^{1/3} \approx 50 \text{ GeV} \left| \frac{3Q_q m_q}{2 \text{ MeV}} \frac{10^{-23} \text{ e cm}}{d_\chi} \right|^{1/3}, \quad (2.15b)$$

where only one flavor quark contribution is assumed. In the above numerical illustration, we have used the model estimation of the LEC constant $c_T = -3.2$ in [34]; there are also other studies that give a smaller magnitude, $c_T \approx -1.0(2)$ [35, 36], which will reduce Λ in Eq. (2.15) by a factor of 0.7. For the flavor symmetric case with $C_{\chi u}^{\text{T1,2}} = C_{\chi d}^{\text{T1,2}} = C_{\chi s}^{\text{T1,2}}$, the μ_χ and d_χ are totally dominated by the strange quark while the contributions from up and down quarks almost cancel out due to the approximate mass relation $m_d \approx 2m_u$.

Now we turn to the matching onto DM-nucleon interactions. First of all, only the single-nucleon currents are present at LO in chiral power counting. The nucleon matrix element of the DM-quark operators can be parameterized in terms of form factors which are restricted by Lorentz covariance, discrete symmetries, and algebraic identities for Dirac matrices and spinors. For the tensor operator, there are three form factors [23],

$$\langle N(k_2) | m_q \bar{q} \sigma^{\mu\nu} q | N(k_1) \rangle = \bar{u}_{k_2} \left[F_{T,0}^{q/N}(q^2) \sigma^{\mu\nu} + F_{T,1}^{q/N}(q^2) \frac{i\gamma^{[\mu} q^{\nu]}}{2m_N} + F_{T,2}^{q/N}(q^2) \frac{iq^{[\mu} k_{12}^{\nu]}}{m_N^2} \right] u_{k_1}, \quad (2.16)$$

where $q^\mu = k_2^\mu - k_1^\mu$, $k_{12}^\mu = k_1^\mu + k_2^\mu$, and m_N is the nucleon mass. In the B χ PT framework, the form factors $F_{T,i}^{q/N}(q^2)$ ($i = 0, 1, 2$) are calculated order by order in the chiral expansion. Owing to the absence of light pseudoscalar poles as well as the small momentum squared of our interest ($|q^2| \sim \mathcal{O}(1 \text{ MeV}^2)$), the form factors can be Taylor-expanded around $q^2 = 0$, with the largest contributions coming from their leading terms. Since the contribution to the DM-nucleon scattering from the $F_{T,2}^{q/N}(0)$ term is suppressed by an additional nucleon

mass relative to the other two, it is a good approximation to keep only $F_{T,0}^{q/N}(0)$ and $F_{T,1}^{q/N}(0)$ for numerical analysis. We employ the following parameterization [37, 38]

$$F_{T,0}^{q/N}(0) = m_q g_T^{q/N}, \quad F_{T,1}^{q/N}(0) = -m_q B_{T,10}^{q/N}(0), \quad (2.17)$$

with the dimensionless parameters $g_T^{q/N}$ and $B_{T,10}^{q/N}(0)$ to be determined. Lattice QCD calculation gives [39]¹

$$g_T^{u/p} = g_T^{d/n} = 0.784(28)(10), \quad g_T^{d/p} = g_T^{u/n} = -0.204(11)(10), \quad g_T^{s/N} = -0.0027(16). \quad (2.18)$$

The form factors $B_{T,10}^{q/N}(0)$ are less well determined and the constituent quark model gives [23, 43]

$$B_{T,10}^{u/p}(0) = B_{T,10}^{d/n}(0) \simeq 3.0, \quad B_{T,10}^{d/p}(0) = B_{T,10}^{u/n}(0) \simeq 0.24, \quad |B_{T,10}^{s/N}(0)| \lesssim 0.2. \quad (2.19)$$

Since the sign of $B_{T,10}^{s/N}(0)$ is not determined yet, we neglect its contribution in our numerical analysis.

To calculate the DM-nucleus matrix element, nonrelativistic (NR)² reduction of the nucleon-level amplitude should be performed to make connections with the treatment in nuclear many-body methods. This is done by taking both the DM and nucleon spinors to the NR limit and expressing the amplitude as a combination of various NR quantities. The NR amplitude can be equivalently obtained using NR operators. In this operator language, according to Eq. (2.16), the chiral LO NR expansions of the contact tensor operators are given by [23],

$$C_{\chi q}^{\text{T1}} \mathcal{O}_{\chi q}^{\text{T1}} \xrightarrow{\text{NR}} 32 C_{\chi q}^{\text{T1}} F_{T,0}^{q/N} m_\chi m_N \mathcal{O}_4^N, \quad (2.20a)$$

$$C_{\chi q}^{\text{T2}} \mathcal{O}_{\chi q}^{\text{T2}} \xrightarrow{\text{NR}} 8 C_{\chi q}^{\text{T2}} \left(m_N F_{T,0}^{q/N} \mathcal{O}_{10}^N - m_\chi (F_{T,0}^{q/N} - F_{T,1}^{q/N}) \mathcal{O}_{11}^N - 4 m_\chi m_N F_{T,0}^{q/N} \mathcal{O}_{12}^N \right), \quad (2.20b)$$

where $F_{T,0(1)}^{q/N} \equiv F_{T,0(1)}^{q/N}(0)$ is used. For the mdm and edm interactions, the NR expansions read

$$\frac{\mu_\chi}{2} (\bar{\chi} \sigma^{\mu\nu} \chi) F_{\mu\nu} \xrightarrow{\text{NR}} -2e\mu_\chi \left[m_N Q_N \mathcal{O}_1^N + 4 \frac{m_\chi m_N}{\mathbf{q}^2} Q_N \mathcal{O}_5^N + 2m_\chi g_N \left(\mathcal{O}_4^N - \frac{\mathcal{O}_6^N}{\mathbf{q}^2} \right) \right], \quad (2.21a)$$

$$\frac{d_\chi}{2} (\bar{\chi} i \sigma^{\mu\nu} \gamma_5 \chi) F_{\mu\nu} \xrightarrow{\text{NR}} -8 \frac{m_\chi m_N}{\mathbf{q}^2} e d_\chi Q_N \mathcal{O}_{11}^N, \quad (2.21b)$$

where Q_N represents the nucleon electric charge in units of e , and g_N is the nucleon Landé g -factor, with $g_p = 5.59$ and $g_n = -3.83$ for the proton and neutron respectively. The involved NR operators in Eq. (2.20) and Eq. (2.21) are [44–46]

$$\mathcal{O}_1^N \equiv \mathbb{1}, \quad \mathcal{O}_4^N \equiv \mathbf{S}_\chi \cdot \mathbf{S}_N, \quad \mathcal{O}_5^N \equiv i \mathbf{S}_\chi \cdot (\mathbf{q} \times \mathbf{v}_N^\perp), \quad \mathcal{O}_6^N \equiv (\mathbf{S}_\chi \cdot \mathbf{q})(\mathbf{S}_N \cdot \mathbf{q}),$$

¹ We find different values of $g_T^{s/N}$ are quoted in the literature. There are two independent lattice calculations, which are consistent, with $g_T^{s/N} = -0.0027(16)$ in [39] and $g_T^{s/N} = -3.19 \times 10^{-3}(69)(2)(22)$ in the erratum to [40] (correcting its first-version value $g_T^{s/N} = -3.2 \times 10^{-4}(24)(0)$). Subsequent quotations made typos; e.g., Refs. [41, 42] quoted $g_T^{s/N} = -0.027(16)$ while Ref. [23] quoted $g_T^{s/N} = (3.2 \pm 8.6) \times 10^{-4}$. The tensor charge $g_T^{s/N}$ is also denoted by δ_s^N in the literature.

²Note that the slight font difference for this abbreviation ‘‘NR’’ and the ‘‘NR’’ used for ‘‘nuclear recoil’’.

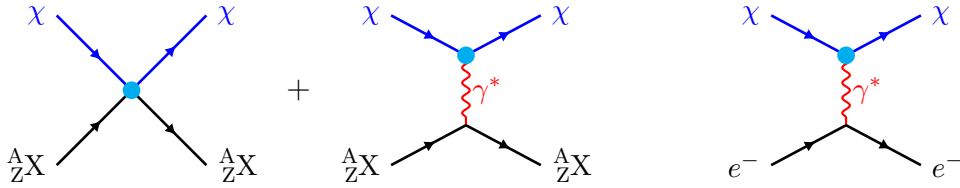


Figure 1. Feynman diagrams for DM-nucleus scattering (the left two diagrams) and DM-electron scattering (the rightmost diagram) induced by $\mathcal{O}_{\chi q}^{\text{T1}}$ and $\mathcal{O}_{\chi q}^{\text{T2}}$.

$$\mathcal{O}_{10}^N \equiv i\mathbf{S}_N \cdot \mathbf{q}, \quad \mathcal{O}_{11}^N \equiv i\mathbf{S}_\chi \cdot \mathbf{q}, \quad \mathcal{O}_{12}^N \equiv \mathbf{v}_N^\perp \cdot (\mathbf{S}_\chi \times \mathbf{S}_N), \quad (2.22)$$

where \mathbf{q} is the three-momentum transfer, and \mathbf{S}_χ and \mathbf{S}_N are respectively the DM and nucleon spin operator. Here the “elastic” transverse velocity is defined by

$$\mathbf{v}_N^\perp \equiv \mathbf{v}_\chi - \frac{\mathbf{q}}{2\mu_{N\chi}}, \quad (2.23)$$

with \mathbf{v}_χ being the incoming DM-nucleon relative velocity and $\mu_{N\chi}$ the reduced mass for the DM-nucleon system.

3 XENON1T constraints

As mentioned in Section 2, $\mathcal{O}_{\chi q}^{\text{T1}}$ and $\mathcal{O}_{\chi q}^{\text{T2}}$ can induce not only 4-fermion DM-nucleon interactions but also the EM dipole moments of the DM. Hereafter, we denote their contribution in DMDD experiments as the short-distance (SD) and long-distance (LD) one respectively. In previous calculations of DMDD constraints on $\mathcal{O}_{\chi q}^{\text{T1}}$ and $\mathcal{O}_{\chi q}^{\text{T2}}$ [11, 20, 21], only the DM-nucleus scattering induced by the SD contribution is considered. A consistent calculation needs to take into account both the SD and LD contributions at the amplitude level, where interference effect between the two is generally expected. In addition to DM-nucleus scattering, the LD dipole operators can also induce DM-electron scattering, as shown in Fig. 1. Due to the excellent potential of DM-electron scattering to probe low-mass DM [17, 18], significant improvements for the constraints in the low-mass region are possible if we take into account the DM-electron scattering induced by the LD dipole contribution.

The XENON1T experiment is a DMDD experiment with a dual-phase time projection chamber, in which both DM-electron and DM-nucleus scattering can induce prompt scintillation photons (S1 signal) and drift electrons (S2 signal) [47]. According to the strength ratio between the S1 and S2 signals, the ER and NR signals can be well distinguished [47]. Comprehensive searches for DM particles have been carried out by the XENON1T collaboration, including NR signals for the DM-nucleus scattering [47], ER signals for the DM-electron scattering [19], and S2-only signals for the Migdal effect [9]. Hereafter, we denote the corresponding constraints from the above three types of signals as the NR, Migdal, and ER constraints respectively. In this section, we utilize the XENON1T experiment as a

benchmark to recalculate the constraints on $\mathcal{O}_{\chi q}^{\text{T1}}$ and $\mathcal{O}_{\chi q}^{\text{T2}}$ with the data given in [9, 19, 47], in which we consistently take into account both the SD and LD contributions.

Our analysis will cover the cases in which the flavor SU(3) symmetry is imposed or not. For the flavor conserving case, a universal Wilson coefficient is assumed for the operators with all of u, d, s quarks; and for the nonconserving case, the contributions from individual flavors are considered separately. The flavor conserving case is adopted in the literature and will serve to compare our results with the existing ones. For convenience, we denote the 90% confidence level (C.L.) constraint on Λ as Λ_q in the flavor conserving case and $\Lambda_u, \Lambda_d, \Lambda_s$ in the nonconserving case. Note that $\mathcal{O}_{\chi q}^{\text{T1}}$ and $\mathcal{O}_{\chi q}^{\text{T2}}$ could also be considered as dimension-six operators if quark masses are removed such that the lower bounds on Λ would be apparently enhanced by a factor of $\sqrt{\Lambda/m_q}$.

3.1 DM-nucleus scattering cross section

In this subsection, we give the differential cross section for the DM-nucleus scattering from the two tensor interactions with both the SD and LD contributions included. The distribution with respect to the nuclear recoil energy E_R ($E_R = \mathbf{q}^2/2m_A$) in the NR limit is given by [42]

$$\frac{d\sigma_T}{dE_R} = \frac{1}{32\pi} \frac{1}{m_\chi^2 m_A} \frac{1}{v^2} \overline{|\mathcal{M}|^2}, \quad (3.1)$$

where m_A is the mass of the target nucleus, v is the speed of the incoming DM particle in the lab frame, and $\overline{|\mathcal{M}|^2}$ is the amplitude squared that has been averaged/summed over the initial/final spin states. The DM-nucleus amplitude \mathcal{M} is given by the sum over all protons and neutrons in the nucleus of the single-nucleon amplitude derived in Section 2. Furthermore, the corresponding NR operators are decomposed into spherical components with a definite angular momentum, which is suitable to computations for a nucleus in an eigenstate of the total angular momentum. By performing a multipole expansion, the unpolarized amplitude squared can be represented in a compact form [42],

$$\overline{|\mathcal{M}|^2} = \frac{m_A^2}{m_N^2} \sum_{i,j} \sum_{N,N'=p,n} f_i^N(\mathbf{q}^2) f_j^{N'}(\mathbf{q}^2) F_{i,j}^{(N,N')}(\mathbf{q}^2, \mathbf{v}_T^{\perp 2}), \quad (3.2)$$

where i and j span the NR operator basis. The squared form factors $F_{i,j}^{(N,N')}(\mathbf{q}^2, \mathbf{v}_T^{\perp 2})$ depend on the nuclear responses as well as \mathbf{q}^2 and $\mathbf{v}_T^{\perp 2} \equiv v^2 - v_{\text{min}}^2$, and the relevant ones in our consideration are collected in Appendix A. Here $v_{\text{min}} = \sqrt{E_R m_A}/(\sqrt{2}\mu_{A\chi})$ is the minimum velocity for DM to induce a nuclear recoil energy E_R with $\mu_{A\chi}$ being the reduced mass for the DM-nucleus system. Detailed formulations of these squared form factors for various nuclei have been provided in [45].

The functions $f_i^N(\mathbf{q}^2)$ are determined by particle physics from the ultraviolet (UV) down to the chiral scale. In our case, they are contributed by both DM-nucleon and

DM dipole interactions induced from the tensor DM-quark operators. Concretely, for the operator $\mathcal{O}_{\chi q}^{\text{T1}}$, the functions that do not vanish are as follows:

$$f_1^N = -2e\mu_\chi m_N Q_N, \quad (3.3a)$$

$$f_4^N = -4e\mu_\chi m_\chi g_N + \sum_{q=u,d,s} 32C_{\chi q}^{\text{T1}} F_{T,0}^{q/N} m_\chi m_N, \quad (3.3b)$$

$$f_5^N = -8e\mu_\chi \frac{m_\chi m_N}{\mathbf{q}^2} Q_N, \quad (3.3c)$$

$$f_6^N = 4e\mu_\chi \frac{m_\chi}{\mathbf{q}^2} g_N. \quad (3.3d)$$

The inclusion of the DM mdm (μ_χ) has resulted in a new term in f_4^N and nonvanishing $f_{1,5,6}^N$. The mdm term in $f_{4,5,6}^N$ will interfere with the usual SD term in f_4^N in the amplitude squared, while f_1^N being DM spin independent will not interfere with $f_{4,5,6}^N$. Similarly, for the operator $\mathcal{O}_{\chi q}^{\text{T2}}$, the nonvanishing functions are

$$f_{10}^N = \sum_{q=u,d,s} 8C_{\chi q}^{\text{T2}} F_{T,0}^{q/N} m_N, \quad (3.4a)$$

$$f_{11}^N = -8 \frac{m_\chi m_N}{\mathbf{q}^2} e d_\chi Q_N - \sum_{q=u,d,s} 8C_{\chi q}^{\text{T2}} (F_{T,0}^{q/N} - F_{T,1}^{q/N}) m_\chi, \quad (3.4b)$$

$$f_{12}^N = - \sum_{q=u,d,s} 32C_{\chi q}^{\text{T2}} F_{T,0}^{q/N} m_\chi m_N. \quad (3.4c)$$

The DM edm leads to an additional term in f_{11}^N , which will interfere with the usual SD term in f_{11}^N and f_{12}^N but not with f_{10}^N as the latter is independent of the DM spin.

3.2 Constraint from NR signals

The differential event rate for NR signals is given by,

$$\frac{dR_{\text{NR}}}{dE_R} = \frac{\rho_\chi}{m_\chi} \frac{1}{m_A} \int_{v_{\min}(E_R)}^{v_{\max}} dv F(v) v \frac{d\sigma_T}{dE_R}(v, E_R), \quad (3.5)$$

where $\rho_\chi = 0.3 \text{ GeV/cm}^3$ is the local DM energy density near the Earth and $F(v)$ is the DM velocity distribution in the lab frame. In the actual calculation, the total rate is a sum of contributions from each isotope weighted by its mass fraction in the nuclear target. Note that the angular distribution of the DM velocity has been integrated out in $F(v)$, since the target nuclei are considered to be at rest and unpolarized in the lab frame.

In the galaxy rest frame, the DM velocity obeys a normal Maxwell-Boltzmann distribution with the circular velocity $v_0 = 220 \text{ km/s}$ [48], which leads to [42, 49]

$$F(v) = \frac{v}{\sqrt{\pi} v_0 v_E} \begin{cases} e^{-(v-v_E)^2/v_0^2} - e^{-(v+v_E)^2/v_0^2}, & \text{for } 0 \leq v \leq v_{\text{esc}} - v_E \\ e^{-(v-v_E)^2/v_0^2} - e^{-v_{\text{esc}}^2/v_0^2}, & \text{for } v_{\text{esc}} - v_E < v \leq v_{\text{esc}} + v_E \end{cases}. \quad (3.6)$$

Here we adopt the averaged Earth relative velocity $v_E = 232$ km/s [50] and the escape velocity $v_{\text{esc}} = 544$ km/s [48], which leads to the maximal DM velocity in the lab frame being $v_{\text{max}} = v_{\text{esc}} + v_E = 776$ km/s.

We calculate the constraint based on the NR events given in [47], for an exposure of $w = 1.0$ ton yr. Taking into account the SM backgrounds, the 90% C.L. constraint is obtained by the criterion of $N_{\text{NR}}^s < 7$ [21], where the number of NR events induced by DM-nucleus scattering is calculated by

$$N_{\text{NR}}^s = w \int_0^{70 \text{ keV}} \epsilon_{\text{NR}}(E_R) \frac{dR_{\text{NR}}}{dE_R} dE_R. \quad (3.7)$$

Here we adopt the NR signal efficiency, $\epsilon_{\text{NR}}(E_R)$, given in Fig. (1) of [47].

The XENON1T constraints on $\mathcal{O}_{\chi q}^{\text{T1}}$ and $\mathcal{O}_{\chi q}^{\text{T2}}$ from NR are shown as red curves in Fig. 2 and Fig. 3. The SD contribution (red dashed curves) dominates over the LD contribution in the constraints on $\mathcal{O}_{\chi q}^{\text{T1}}$ for the valence u and d quarks. For the sea s quark, the SD contribution is relatively less important than the LD one (red dotted curves) for small m_χ until $m_\chi \gtrsim 50$ GeV when their constructive interference starts to become significant. Regarding the constraints on $\mathcal{O}_{\chi q}^{\text{T2}}$, the LD contribution dominates overwhelmingly for the s quark, while the u and d quarks exhibit comparable but varying contributions from the SD and LD mechanisms. Note that the interference effect is constructive (destructive) in the u (d) quark scenario. This distinct behavior is due to the charge sign difference between the u and d quarks. For both operators $\mathcal{O}_{\chi q}^{\text{T1}}$ and $\mathcal{O}_{\chi q}^{\text{T2}}$ in the flavor conserving case, the constraint from SD is dominated by the d quark contribution while the LD constraint is dominated by the s quark contribution. Especially for $\mathcal{O}_{\chi q}^{\text{T2}}$, the LD contribution always dominates, but becomes comparable with the SD one for a large m_χ where a significant destructive interference pattern is evident in the full constraint (red solid curve).

3.3 Constraint from the Migdal effect

In the DM low-mass region (i.e. sub-GeV region) the constraint from NR signals loses sensitivity since the nucleus cannot gain enough recoil energy to reach the threshold of a detector. This dilemma can be alleviated by taking advantage of the Migdal effect. In addition to the NR signals from DM-nucleus scattering, the Migdal effect results in additional ionization energy E_{EM} deposited in the detector so that the total detected energy is $E_{\text{det}} = \mathcal{L}E_R + E_{\text{EM}}$. Unlike the ER, a large fraction of NR energy becomes unobservable heat. Here \mathcal{L} is the quenching factor for the NR signals, which accounts for the fraction of NR energy converting into photoelectric signals. In calculations of the Migdal effect, it has become customary to take a constant value of $\mathcal{L} = 0.15$ [51].

Taking into account the Migdal effect for the DM-nucleus scattering, one needs to attach an additional ionization form factor to Eq. (3.5) to obtain the differential event

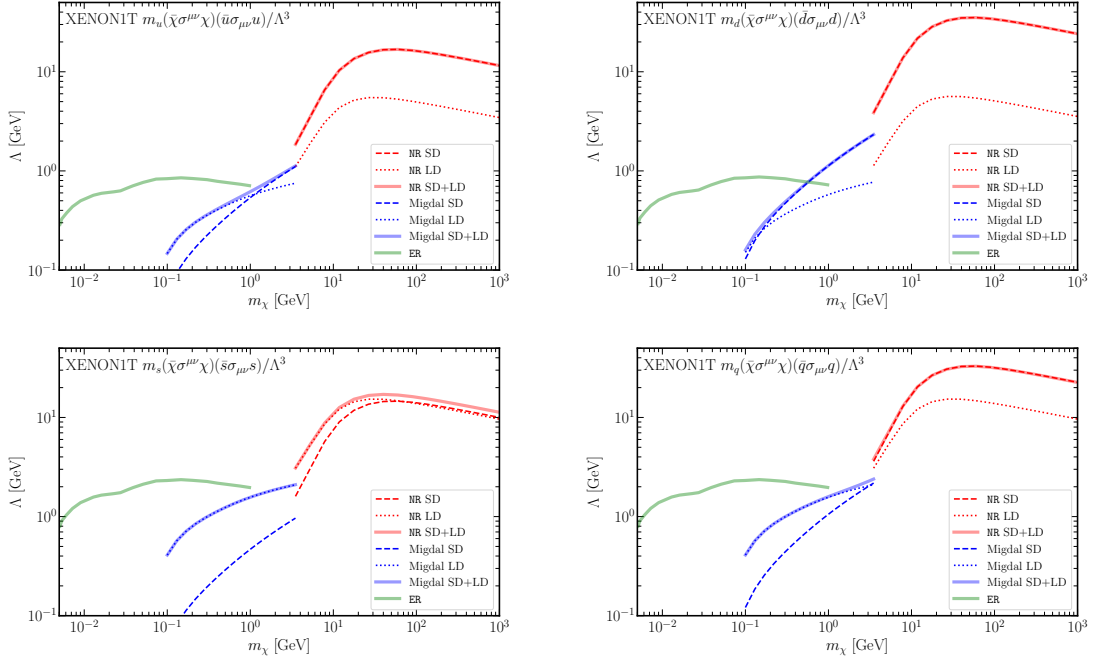


Figure 2. XENON1T constraints on $\mathcal{O}_{\chi q}^{\text{T1}}$ from NR signals (red), the Migdal effect (blue), and ER signals (green). For the NR and the Migdal effect cases, we consider the constraints with SD-only (dashed), LD-only (dotted), and full (solid) contributions respectively. For the ER case, only the LD contribution is involved. In the top two and the bottom left panels, contributions from u , d , and s quarks are taken into account separately. In the bottom right panel, a flavor universal coupling is assumed for u , d , and s quarks.

rate, namely [7]

$$\frac{dR_{\text{Migdal}}}{dE_{\text{det}}} = \frac{\rho_{\chi}}{m_{\chi}} \frac{1}{m_A} \int_0^{E_R^{\text{max}}} dE_R \int_{v_{\text{min}}}^{v_{\text{max}}} dv F(v) v \frac{d\sigma_T}{dE_R}(v, E_R) |Z_{\text{ion}}(E_R, E_{\text{EM}})|^2, \quad (3.8)$$

where $E_R^{\text{max}} = 2\mu_{A\chi}^2 v_{\text{max}}^2 / m_A$ and $E_{\text{EM}} = E_{\text{det}} - \mathcal{L}E_R$. Unlike the NR case, here $v_{\text{min}} = (m_A E_R + \mu_{A\chi} E_{\text{EM}}) / (\mu_{A\chi} \sqrt{2m_A E_R})$ depends on not only the NR energy E_R but also the ionization energy E_{EM} . The ionization factor $|Z_{\text{ion}}|^2$ also depends on both, which is given by [7],

$$|Z_{\text{ion}}|^2 = \frac{1}{2\pi} \sum_{n,\ell} \frac{d}{dE_e} p_{q_e}^c(n\ell \rightarrow E_e), \quad (3.9)$$

where E_e is the kinetic energy of the ionized electron given by $E_e = E_{\text{EM}} - |E_{n\ell}|$, with $|E_{n\ell}|$ being the binding energy of the electron labeled by the principal and orbital quantum numbers n, ℓ . We adopt the ionization probability $p_{q_e}^c$ of the Xenon atom given in [7].

For the Migdal effect, we calculate the constraint with the S2-only data set given in [9, 52] for an exposure of $w = 22$ ton-day. The 90% C.L. constraint is obtained via the

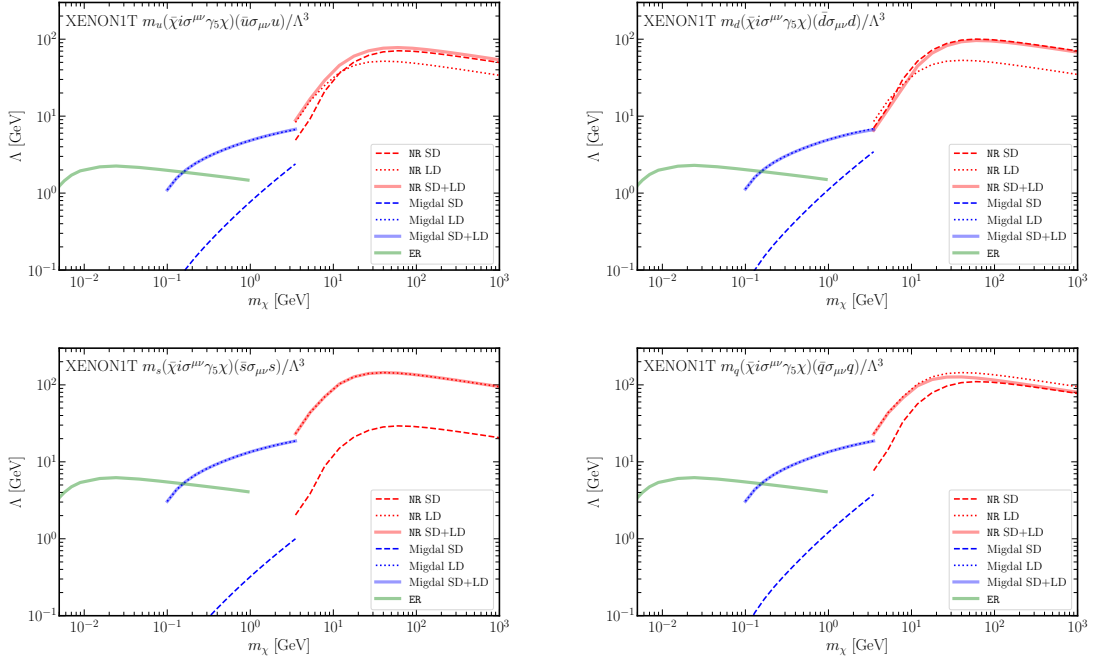


Figure 3. Same as Fig. 2 but for the operator $\mathcal{O}_{\chi q}^{\text{T2}}$.

criterion of $N_{\text{Migdal}}^s < 49$ [11, 51], where the number of signal events induced by the Migdal effect is calculated by

$$N_{\text{Migdal}}^s = w \int_{0.186 \text{ keV}}^{3.90 \text{ keV}} \epsilon_{\text{Migdal}}(E_{\text{det}}) \frac{dR_{\text{Migdal}}}{dE_{\text{det}}}. \quad (3.10)$$

Here we adopt the signal efficiency of the S2-only data, $\epsilon_{\text{Migdal}}(E_{\text{det}})$, given in [9, 52].

The XENON1T constraints on $\mathcal{O}_{\chi q}^{\text{T1}}$ and $\mathcal{O}_{\chi q}^{\text{T2}}$ from the Migdal effect are shown as blue curves in Fig. 2 and Fig. 3. Upon including the LD contribution, the constraints on $\mathcal{O}_{\chi q}^{\text{T2}}$ achieve a significant enhancement, particularly for Λ_s , by a factor up to two orders of magnitude. As for the constraints on $\mathcal{O}_{\chi q}^{\text{T1}}$, there exist mass regions where the SD and LD contributions are comparable for the u and d quarks, in which the SD and LD contributions have constructive interference.

3.4 Constraint from ER signals

The constraints on the edm and mDM of DM from ER signals have been carried out by the XENON1T collaboration [19], in which S2-only signals induced by a single electron are used to achieve a lower energy threshold. For the DM-electron scattering induced by $\mathcal{O}_{\chi q}^{\text{T1}}$ and $\mathcal{O}_{\chi q}^{\text{T2}}$, there is only LD contribution. Hence, we can directly convert these constraints on DM dipole moments into those on $\mathcal{O}_{\chi q}^{\text{T1}}$ and $\mathcal{O}_{\chi q}^{\text{T2}}$ via Eq. (2.15).

The XENON1T constraints on $\mathcal{O}_{\chi q}^{\text{T1}}$ and $\mathcal{O}_{\chi q}^{\text{T2}}$ from ER are shown as green curves in Fig. 2 and Fig. 3. These ER constraints effectively probe low-mass DM down to approximately

5 MeV. The small momentum transfer in DM-electron scattering for such low-mass DM results in an enhanced scattering cross section when DM interacts with electrons via edm, leading to a stronger constraint on $\mathcal{O}_{\chi q}^{\text{T2}}$ compared to $\mathcal{O}_{\chi q}^{\text{T1}}$. Moreover, the constraints on Λ_s are more stringent than those on Λ_u and Λ_d due to the quark mass factor in the definition of $\mathcal{O}_{\chi q}^{\text{T1}}$ ($\mathcal{O}_{\chi q}^{\text{T2}}$). For the flavor conserving case, the constraints on both operators from Migdal effect and ER are similar to those in the single strange quark case, since they are dominated by LD contributions which are further enhanced by the strange mass.

The stronger constraint on $\mathcal{O}_{\chi q}^{\text{T2}}$ can be understood as follows. In the nonrelativistic limit, the spin-averaged and -summed matrix element squared of the DM-electron scattering for the mdm and edm cases are

$$\overline{|\mathcal{M}_{\chi e}(q)|^2}_{\text{mdm}} \simeq 16\pi\alpha\mu_\chi^2 m_\chi^2, \quad \overline{|\mathcal{M}_{\chi e}(q)|^2}_{\text{edm}} \simeq 64\pi\alpha d_\chi^2 m_\chi^2 m_e^2 / q^2. \quad (3.11)$$

Here q is the momentum transfer in DM-electron scattering and has a typical value of $q \simeq \alpha m_e$ in DMDD experiments. At such a low momentum transfer scale, $\overline{|\mathcal{M}_{\chi e}(q)|^2}_{\text{edm}}$ is enhanced by a factor of α , namely, $\overline{|\mathcal{M}_{\chi e}(\alpha m_e)|^2}_{\text{edm}} \simeq 64\pi d_\chi^2 m_\chi^2 / \alpha$, which thus leads to a stronger constraint on the edm of DM, as compared to the mdm of DM.

4 Constraints from other DMDD experiments

Besides the XENON1T experiment [19], constraints on DM EM dipole moments are also derived in XENON10 and DarkSide50 via ER signals [22] and PandaX via NR signals [53]. Hence, it is instructive to recast these constraints via Eq. (2.15) to fully constrain the two tensor operators, $\mathcal{O}_{\chi q}^{\text{T1}}$ and $\mathcal{O}_{\chi q}^{\text{T2}}$.³ Together with the constraints from XENON1T calculated above, we show in Fig. 4 all the available bounds on $\mathcal{O}_{\chi q}^{\text{T1}}$ and $\mathcal{O}_{\chi q}^{\text{T2}}$ obtained in this work by colored curves. Here we only show the results for the flavor conserving case to facilitate comparison with the results in the literature (represented by dashed gray curves for the NR [21] and the Migdal effect [11]), in which only the SD contribution is considered.⁴

By taking advantage of the new LD contribution, $\mathcal{O}_{\chi q}^{\text{T1}}$ and $\mathcal{O}_{\chi q}^{\text{T2}}$ can also be constrained by ER, in addition to NR and the Migdal effect. These new ER constraints cover a previously uncovered low-mass region with $5 \text{ MeV} \lesssim m_\chi \lesssim 100 \text{ MeV}$ and surpass the previous constraints from the Migdal effect in the mass region, $100 \text{ MeV} \lesssim m_\chi \lesssim 1 \text{ GeV}$. Owing to the enhancement of the LD contribution at the small momentum transfer in the Migdal effect, the newly calculated XENON1T constraint from the Migdal effect is stronger than the previous one from the Migdal effect by about a factor of three (one order of magnitude)

³Note that a consistent calculation on the constraint from PandaX NR also needs to consider the SD contribution, as we did with XENON1T NR in the previous section. For simplicity, we restrict our discussion here to the LD contribution only.

⁴To cross check our calculations, we attempted to reproduce the XENON1T constraints in [11] on the two DM-quark tensor operators from the Migdal effect. We found that we could get results consistent with [11] only when we adopted the mistaken value of $g_T^{s/N} = -0.027$, as discussed in footnote 1.

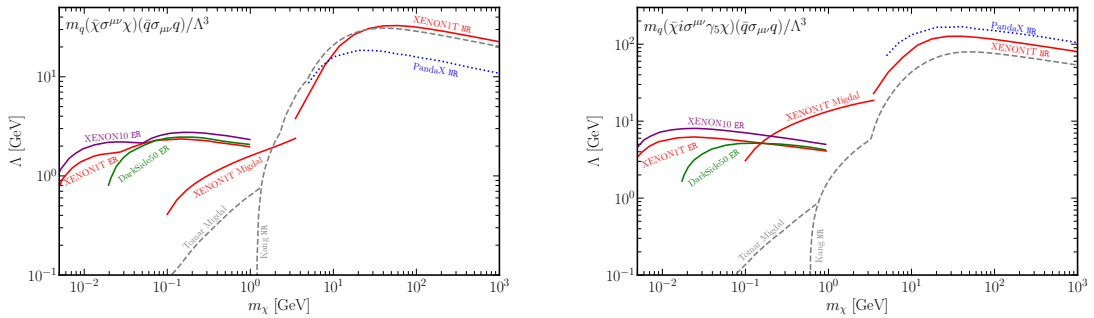


Figure 4. Constraints on $\mathcal{O}_{\chi q}^{T1}$ (left panel) and $\mathcal{O}_{\chi q}^{T2}$ (right panel) for the flavor conserving case from current DMDD experiments. Colored lines show new constraints in this work with the LD contribution included. Two gray dashed curves show existing constraints from NR [21] and the Migdal effect [11], in which only the SD contribution is considered. The legends follow those in Fig. 2 and Fig. 3: the dashed, dotted, and solid curves indicate the constraints with SD-only, LD-only, and full contributions respectively.

in the $\mathcal{O}_{\chi q}^{T1}$ ($\mathcal{O}_{\chi q}^{T2}$) case. In particular, for the $\mathcal{O}_{\chi q}^{T2}$ case, the XENON1T constraint from the Migdal effect can be even stronger than the previous ones from NR in the mass region of $0.7 \text{ GeV} \lesssim m_\chi \lesssim 3 \text{ GeV}$. Due to the relatively large momentum transfer in NR, the improvements in the constraints from NR are not so obvious, compared to those from the Migdal effect. For the $\mathcal{O}_{\chi q}^{T2}$ case, the PandaX constraint from NR improves in the large mass region ($m_\chi \gtrsim 3 \text{ GeV}$). But it is expected to become slightly weaker for heavier DM when the SD contribution is also considered because of the destructive interference between the LD and SD contributions as shown in Fig. 3.

5 Conclusion

In this work, we offered a more complete investigation of the two DM-quark tensor operators in dark matter direct detection (DMDD) experiments in the framework of chiral perturbation theory. We found that DM-quark tensor operators can induce electromagnetic dipole moment operators of the DM, in addition to the well-studied DM-nucleon 4-fermion operators. In previous calculations for DMDD experiments, the constraints on DM-quark tensor operators were obtained by calculating the NR and the Migdal effect induced by these 4-fermion operators. The DM dipole moment operators can give rise to new contributions for both DM-electron and DM-nucleus scatterings. Consequently, a consistent calculation of the constraints from the NR and Migdal effect should include both DM-nucleon and DM dipole moment operators, which may result in interesting interference effects. Remarkably, the DM-quark tensor operators can also be constrained by ER signals caused by the newly generated DM-electron scattering. In this manner we derived the constraints from the NR and the Migdal effect using the XENON1T data, and recast the existing bounds from the

ER (XENON10, XENON1T, DarkSide50) and NR (PandaX) signals to yield comprehensive constraints on the tensor interactions. Our results have significantly improved over the previous ones in the literature, especially in the sub-GeV region.

Acknowledgments

This work was supported in part by the Guangdong Major Project of Basic and Applied Basic Research No. 2020B0301030008, and by the Grants No. NSFC-12035008, No. NSFC-12247151, No. NSFC-12305110, and No. NSFC-12347121.

A Squared form factor

The squared form factors $F_{i,j}^{(N,N')}(\mathbf{q}^2, \mathbf{v}_T^{\perp 2})$ defined in Eq. (3.2) are related to the basic independent nuclear form factors in the following way [45],

$$F_{1,1}^{(N,N')} = F_M^{(N,N')}, \quad (\text{A.1})$$

$$F_{4,4}^{(N,N')} = \frac{1}{16} \left(F_{\Sigma'}^{(N,N')} + F_{\Sigma''}^{(N,N')} \right), \quad (\text{A.2})$$

$$F_{5,5}^{(N,N')} = \frac{\mathbf{q}^2}{4} \left(\mathbf{v}_T^{\perp 2} F_M^{(N,N')} + \frac{\mathbf{q}^2}{m_N^2} F_{\Delta}^{(N,N')} \right), \quad (\text{A.3})$$

$$F_{6,6}^{(N,N')} = \frac{\mathbf{q}^4}{16} F_{\Sigma''}^{(N,N')}, \quad (\text{A.4})$$

$$F_{4,5}^{(N,N')} = -\frac{\mathbf{q}^2}{8m_N} F_{\Sigma',\Delta}^{(N,N')}, \quad (\text{A.5})$$

$$F_{4,6}^{(N,N')} = \frac{\mathbf{q}^2}{16} F_{\Sigma''}^{(N,N')}, \quad (\text{A.6})$$

$$F_{10,10}^{(N,N')} = \frac{\mathbf{q}^2}{4} F_{\Sigma''}^{(N,N')}, \quad (\text{A.7})$$

$$F_{11,11}^{(N,N')} = \frac{\mathbf{q}^2}{4} F_M^{(N,N')}, \quad (\text{A.8})$$

$$F_{12,12}^{(N,N')} = \frac{\mathbf{v}_T^{\perp 2}}{16} \left(\frac{1}{2} F_{\Sigma'}^{(N,N')} + F_{\Sigma''}^{(N,N')} \right) + \frac{\mathbf{q}^2}{16m_N^2} \left(F_{\Phi'}^{(N,N')} + F_{\Phi''}^{(N,N')} \right), \quad (\text{A.9})$$

$$F_{11,12}^{(N,N')} = -\frac{\mathbf{q}^2}{8m_N} F_{M,\Phi''}^{(N,N')}. \quad (\text{A.10})$$

References

- [1] G. Bertone, D. Hooper and J. Silk, *Particle dark matter: Evidence, candidates and constraints*, *Phys. Rept.* **405** (2005) 279–390, [[hep-ph/0404175](#)].
- [2] J. L. Feng, *Dark Matter Candidates from Particle Physics and Methods of Detection*, *Ann. Rev. Astron. Astrophys.* **48** (2010) 495–545, [[1003.0904](#)].
- [3] L. Roszkowski, E. M. Sessolo and S. Trojanowski, *WIMP dark matter candidates and searches—current status and future prospects*, *Rept. Prog. Phys.* **81** (2018) 066201, [[1707.06277](#)].

- [4] M. Schumann, *Direct Detection of WIMP Dark Matter: Concepts and Status*, *J. Phys. G* **46** (2019) 103003, [[1903.03026](#)].
- [5] C. Kouvaris and J. Pradler, *Probing sub-GeV Dark Matter with conventional detectors*, *Phys. Rev. Lett.* **118** (2017) 031803, [[1607.01789](#)].
- [6] A. B. Migdal, *Ionization of atoms accompanying α - and β -decay*, *J. Phys.* *4*, 449 (1941) (1941) .
- [7] M. Ibe, W. Nakano, Y. Shoji and K. Suzuki, *Migdal Effect in Dark Matter Direct Detection Experiments*, *JHEP* **03** (2018) 194, [[1707.07258](#)].
- [8] LUX collaboration, D. S. Akerib et al., *Results of a Search for Sub-GeV Dark Matter Using 2013 LUX Data*, *Phys. Rev. Lett.* **122** (2019) 131301, [[1811.11241](#)].
- [9] XENON collaboration, E. Aprile et al., *Search for Light Dark Matter Interactions Enhanced by the Migdal Effect or Bremsstrahlung in XENON1T*, *Phys. Rev. Lett.* **123** (2019) 241803, [[1907.12771](#)].
- [10] EDELWEISS collaboration, E. Armengaud et al., *Searching for low-mass dark matter particles with a massive Ge bolometer operated above-ground*, *Phys. Rev. D* **99** (2019) 082003, [[1901.03588](#)].
- [11] G. Tomar, S. Kang and S. Scopel, *Low-mass extension of direct detection bounds on WIMP-quark and WIMP-gluon effective interactions using the Migdal effect*, *Astropart. Phys.* **150** (2023) 102851, [[2210.00199](#)].
- [12] DARKSIDE collaboration, P. Agnes et al., *Search for Dark-Matter–Nucleon Interactions via Migdal Effect with DarkSide-50*, *Phys. Rev. Lett.* **130** (2023) 101001, [[2207.11967](#)].
- [13] SUPERCDMS collaboration, M. F. Albakry et al., *Search for low-mass dark matter via bremsstrahlung radiation and the Migdal effect in SuperCDMS*, *Phys. Rev. D* **107** (2023) 112013, [[2302.09115](#)].
- [14] C. V. Cappiello, K. C. Y. Ng and J. F. Beacom, *Reverse Direct Detection: Cosmic Ray Scattering With Light Dark Matter*, *Phys. Rev. D* **99** (2019) 063004, [[1810.07705](#)].
- [15] T. Bringmann and M. Pospelov, *Novel direct detection constraints on light dark matter*, *Phys. Rev. Lett.* **122** (2019) 171801, [[1810.10543](#)].
- [16] Y. Kahn and T. Lin, *Searches for light dark matter using condensed matter systems*, *Rept. Prog. Phys.* **85** (2022) 066901, [[2108.03239](#)].
- [17] R. Essig, J. Mardon and T. Volansky, *Direct Detection of Sub-GeV Dark Matter*, *Phys. Rev. D* **85** (2012) 076007, [[1108.5383](#)].
- [18] R. Essig, A. Manalaysay, J. Mardon, P. Sorensen and T. Volansky, *First Direct Detection Limits on sub-GeV Dark Matter from XENON10*, *Phys. Rev. Lett.* **109** (2012) 021301, [[1206.2644](#)].
- [19] XENON collaboration, E. Aprile et al., *Emission of single and few electrons in XENON1T and limits on light dark matter*, *Phys. Rev. D* **106** (2022) 022001, [[2112.12116](#)].
- [20] S. Kang, S. Scopel, G. Tomar and J.-H. Yoon, *Present and projected sensitivities of Dark*

- Matter direct detection experiments to effective WIMP-nucleus couplings*, *Astropart. Phys.* **109** (2019) 50–68, [[1805.06113](#)].
- [21] S. Kang, S. Scopel, G. Tomar and J.-H. Yoon, *On the sensitivity of present direct detection experiments to WIMP–quark and WIMP–gluon effective interactions: A systematic assessment and new model–independent approaches*, *Astropart. Phys.* **114** (2020) 80–91, [[1810.00607](#)].
- [22] R. Catena, T. Emken, N. A. Spaldin and W. Tarantino, *Atomic responses to general dark matter–electron interactions*, *Phys. Rev. Res.* **2** (2020) 033195, [[1912.08204](#)].
- [23] F. Bishara, J. Brod, B. Grinstein and J. Zupan, *From quarks to nucleons in dark matter direct detection*, *JHEP* **11** (2017) 059, [[1707.06998](#)].
- [24] W. Dekens, E. E. Jenkins, A. V. Manohar and P. Stoffer, *Non-perturbative effects in $\mu \rightarrow e\gamma$* , *JHEP* **01** (2019) 088, [[1810.05675](#)].
- [25] F.-Z. Chen, M.-D. Zheng and H.-H. Zhang, *Nonperturbative effects in neutrino magnetic moments*, *Phys. Rev. D* **106** (2022) 095009, [[2206.13122](#)].
- [26] J. Brod, A. Gootjes-Dreesbach, M. Tamaro and J. Zupan, *Effective Field Theory for Dark Matter Direct Detection up to Dimension Seven*, *JHEP* **10** (2018) 065, [[1710.10218](#)].
- [27] J. Goodman, M. Ibe, A. Rajaraman, W. Shepherd, T. M. P. Tait and H.-B. Yu, *Constraints on Dark Matter from Colliders*, *Phys. Rev. D* **82** (2010) 116010, [[1008.1783](#)].
- [28] T. Li, X.-D. Ma, M. A. Schmidt and R.-J. Zhang, *The implication of $J/\psi \rightarrow (\gamma+)$ invisible for the effective field theories of neutrino and dark matter*, *Phys. Rev. D* **104** (2021) 035024, [[2104.01780](#)].
- [29] J.-H. Liang, Y. Liao, X.-D. Ma and H.-L. Wang, *Dark sector effective field theory*, *JHEP* **12** (2023) 172, [[2309.12166](#)].
- [30] F. Bishara, J. Brod, B. Grinstein and J. Zupan, *Chiral Effective Theory of Dark Matter Direct Detection*, *JCAP* **02** (2017) 009, [[1611.00368](#)].
- [31] O. Cata and V. Mateu, *Chiral perturbation theory with tensor sources*, *JHEP* **09** (2007) 078, [[0705.2948](#)].
- [32] J. Gasser and H. Leutwyler, *Chiral Perturbation Theory to One Loop*, *Annals Phys.* **158** (1984) 142.
- [33] J. Gasser and H. Leutwyler, *Chiral Perturbation Theory: Expansions in the Mass of the Strange Quark*, *Nucl. Phys. B* **250** (1985) 465–516.
- [34] V. Mateu and J. Portoles, *Form-factors in radiative pion decay*, *Eur. Phys. J. C* **52** (2007) 325–338, [[0706.1039](#)].
- [35] I. Baum, V. Lubicz, G. Martinelli, L. Orifici and S. Simula, *Matrix elements of the electromagnetic operator between kaon and pion states*, *Phys. Rev. D* **84** (2011) 074503, [[1108.1021](#)].
- [36] G. Ecker, J. Gasser, A. Pich and E. de Rafael, *The Role of Resonances in Chiral Perturbation Theory*, *Nucl. Phys. B* **321** (1989) 311–342.

- [37] QCDSF, UKQCD collaboration, M. Gockeler, P. Hagler, R. Horsley, D. Pleiter, P. E. L. Rakow, A. Schafer et al., *Quark helicity flip generalized parton distributions from two-flavor lattice QCD*, *Phys. Lett. B* **627** (2005) 113–123, [[hep-lat/0507001](#)].
- [38] M. Diehl, *Generalized parton distributions with helicity flip*, *Eur. Phys. J. C* **19** (2001) 485–492, [[hep-ph/0101335](#)].
- [39] R. Gupta, B. Yoon, T. Bhattacharya, V. Cirigliano, Y.-C. Jang and H.-W. Lin, *Flavor diagonal tensor charges of the nucleon from (2+1+1)-flavor lattice QCD*, *Phys. Rev. D* **98** (2018) 091501, [[1808.07597](#)].
- [40] C. Alexandrou et al., *Nucleon scalar and tensor charges using lattice QCD simulations at the physical value of the pion mass*, *Phys. Rev. D* **95** (2017) 114514, [[1703.08788](#)].
- [41] FLAVOUR LATTICE AVERAGING GROUP collaboration, S. Aoki et al., *FLAG Review 2019: Flavour Lattice Averaging Group (FLAG)*, *Eur. Phys. J. C* **80** (2020) 113, [[1902.08191](#)].
- [42] E. Del Nobile, *The Theory of Direct Dark Matter Detection: A Guide to Computations*, [2104.12785](#).
- [43] B. Pasquini, M. Pincetti and S. Boffi, *Chiral-odd generalized parton distributions in constituent quark models*, *Phys. Rev. D* **72** (2005) 094029, [[hep-ph/0510376](#)].
- [44] E. Del Nobile, *Complete Lorentz-to-Galileo dictionary for direct dark matter detection*, *Phys. Rev. D* **98** (2018) 123003, [[1806.01291](#)].
- [45] A. L. Fitzpatrick, W. Haxton, E. Katz, N. Lubbers and Y. Xu, *The Effective Field Theory of Dark Matter Direct Detection*, *JCAP* **02** (2013) 004, [[1203.3542](#)].
- [46] N. Anand, A. L. Fitzpatrick and W. C. Haxton, *Weakly interacting massive particle-nucleus elastic scattering response*, *Phys. Rev. C* **89** (2014) 065501, [[1308.6288](#)].
- [47] XENON collaboration, E. Aprile et al., *Dark Matter Search Results from a One Ton-Year Exposure of XENON1T*, *Phys. Rev. Lett.* **121** (2018) 111302, [[1805.12562](#)].
- [48] M. C. Smith et al., *The RAVE Survey: Constraining the Local Galactic Escape Speed*, *Mon. Not. Roy. Astron. Soc.* **379** (2007) 755–772, [[astro-ph/0611671](#)].
- [49] J. D. Lewin and P. F. Smith, *Review of mathematics, numerical factors, and corrections for dark matter experiments based on elastic nuclear recoil*, *Astropart. Phys.* **6** (1996) 87–112.
- [50] W. Wang, K.-Y. Wu, L. Wu and B. Zhu, *Direct detection of spin-dependent sub-GeV dark matter via Migdal effect*, *Nucl. Phys. B* **983** (2022) 115907, [[2112.06492](#)].
- [51] N. F. Bell, J. B. Dent, B. Dutta, S. Ghosh, J. Kumar and J. L. Newstead, *Low-mass inelastic dark matter direct detection via the Migdal effect*, *Phys. Rev. D* **104** (2021) 076013, [[2103.05890](#)].
- [52] XENON collaboration, E. Aprile et al., *Light Dark Matter Search with Ionization Signals in XENON1T*, *Phys. Rev. Lett.* **123** (2019) 251801, [[1907.11485](#)].
- [53] PANDAX collaboration, X. Ning et al., *Limits on the luminance of dark matter from xenon recoil data*, *Nature* **618** (2023) 47–50.